



Influence of the coiling porosity on the risk reduction of the cerebral aneurysm rupture: computational study

Downloaded from: <https://research.chalmers.se>, 2025-12-05 03:27 UTC

Citation for the original published paper (version of record):

Sheidani, A., Barzegar Gerdroodbary, M., Poozesh, A. et al (2022). Influence of the coiling porosity on the risk reduction of the cerebral aneurysm rupture: computational study. *Scientific Reports*, 12(1). <http://dx.doi.org/10.1038/s41598-022-23745-1>

N.B. When citing this work, cite the original published paper.



OPEN

Influence of the coiling porosity on the risk reduction of the cerebral aneurysm rupture: computational study

Armin Sheidani¹, M. Barzegar Gerdroodbary^{2✉}, Amin Poozesh³, Amir Sabernaemi⁴, Sajad Salavatidezfouli⁵ & Arash Hajisharifi⁵

The formation and progress of cerebral aneurysm is highly associated with hemodynamic factors and blood flow feature. In this study, comprehensive efforts are done to investigate the blood hemodynamic effects on the creation and growth of the Internal Carotid Artery. The computational fluid dynamic method is used for the visualization of the bloodstream inside the aneurysm. Transitional, non-Newtonian and incompressible conditions are considered for solving the Navier–Stokes equation to achieve the high-risk region on the aneurysm wall. OSI and WSS of the aneurysm wall are compared within different blood flow stages. The effects of blood viscosity and coiling treatment on these factors are presented in this work. Our study shows that in male patients (HCT = 0.45), changing the porosity of coiling from 0.89 with 0.79 would decrease maximum OSI up to 75% (in maximum acceleration). However, this effect is limited to about 45% for female patients (HCT = 0.35).

The major cause of premature and abnormalities deaths throughout the world is Cardiovascular diseases (CVDs). World Health Organization (WHO) reported that annual death related to CVDS is about 18 million peoples and this disease is known as the main threat for human life in the future. Among the different CVDs, a Cerebral Aneurysm (CA) is a conventional disease which causes severe unwanted effect on human life^{1,2}. A Cerebral Aneurysm (CA) is a thin or weak sac on an artery in the brain that bulges or balloons out and fills with blood and 3–5% of peoples has this disorder. An intracranial or cerebral aneurysm is an unusual main enlargement of an artery in the brain and it is mainly initiated when the internal muscular layer of a blood vessel wall becomes weak^{3,4}. The rupture of this arterial wall threatening the human life by coma, stroke or death. Although significant advances have been achieved in surgical techniques, high rates of death were reported by aneurysm rupture in recent years.

The endovascular coiling and microsurgical clipping are current treatment selections and both of them have side effects and high risk^{5–7}. Available resource show that the size of most CA is small and about 70% of these CA did not rupture. Researchers have reported that the aneurysmal dilatation at the apex and local weakness are the main reasons for the formation of the CA. A finite element application of arterial wall evolution and remodelling with application to abdominal aortic aneurysms were done to investigate the risk of this disorder^{8–10}. Because of the impingement of main blood stream, hemodynamic force applied on the artery and this is significant factor for degradation of the flexible membrane. Although Intracranial aneurysms have been recognized as a system of rare family, they are not known as sporadic wounds.

Three main treatments for this disease are clipping, coiling and stenting. Due to surgical issue, the first treatment is not always used. In fact, clipping is widely replaced by the coiling technique. Besides, the selection of the treatment technique is mainly done over the analysis of the geometrical aspects of aneurysm^{11,12}. Meanwhile, aneurysm conditions and locations are also considered for the evaluation of the treatment. In Guglielmi Detachable Coil (GDC) procedure, endovascular coiling is done by an interventional neuro-radiologist with high skill in interventional radiology. Although the ratio of accomplishment in clipping technique is higher than in coiling, some difficulties, such as, haemorrhage, bleeding, high risk, and incomplete occlusion coiling does not happen by

¹Mechanical Engineering Department, Politecnico di Milano, Milan, Italy. ²Department of Mechanical Engineering, Babol Noshirvani University of Technology, Babol, Iran. ³Department of Aerospace Engineering, K.N. Toosi University of Technology, Tehran, Iran. ⁴Department of Space, Earth and Environment, Chalmers University of Technology, Gothenburg, Sweden. ⁵Mathematics Area, MathLab, International School for Advanced Studies (SISSA), Trieste, Italy. ✉email: mbarzegarg@yahoo.com

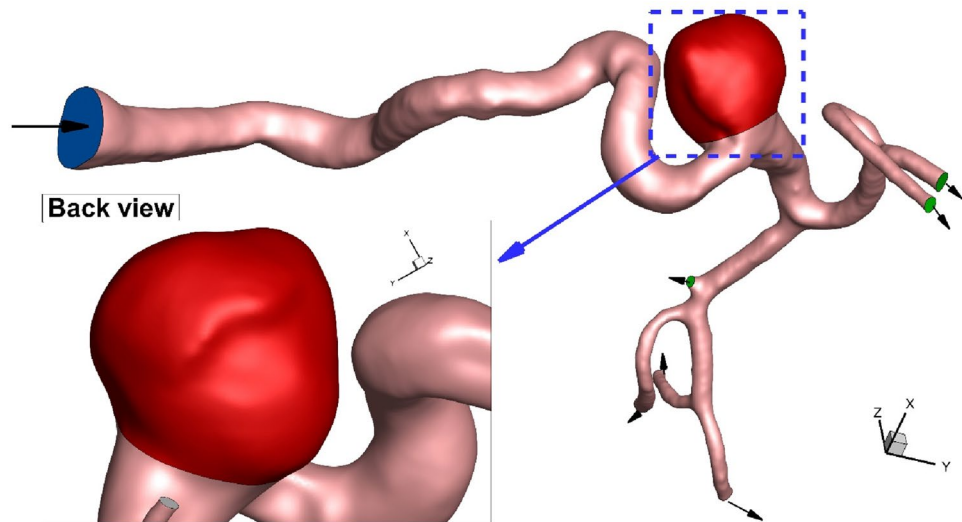


Figure 1. ICA aneurysm.

application of coiling. In fact, surgeons could manage the coil inside the aneurysms^{13,14}. After inserting the coil inside the aneurysm, light electricity is streamed in the coil. Although this technique seems efficient for aneurysm treatments, there are still some disadvantages and it is not recommended for the aneurysm with wide neck.

Due to importance of the aneurysm feature, hemodynamic analysis of the blood stream within the cerebral aneurysm becomes important. In fact, the diagnosis of the high risk section on the wall of the aneurysm is highly significant for the coiling process. It should be considered that the blood stream inside the arteries follows the rhythm of heart pulse and this has high influence on the growth and rupture of the aneurysms. Although several works have been developed for the hemodynamic study of the blood stream inside the aneurysms^{15–17}, the most previous works just select superficial aneurysm model for case studies. Meanwhile, correct characteristics of blood stream is not also considered for their evaluations.

In current work, hemodynamic features of the blood stream inside the real cerebral aneurysm have been investigated to diagnose the main factors for the progress of the aneurysm and/or its rupture (Fig. 1). Computational fluid dynamic (CFD) is used for simulation of the blood flow. The effective of pulse blood flow is also considered in this work by transient study of the blood stream. The effects of the blood viscosity and coiling percentage inside the aneurysm are also investigated. Wall shear stress and OSI are also compared in different blood flow rate to find the high-risk region for rupture.

Applied technique for modelling

The computational study of the blood stream inside the artery is done via CFD method. Navier–Stokes equations are solved while it assumed that blood flow is transient, incompressible and non-Newtonian¹⁸. Casson model is used for the estimation of blood viscosity and stress on aneurysm wall with haematocrit value of 40%. The selected aneurysm (internal carotid artery) geometry is obtained from Emory University and details are available in Ref.¹⁹. Since the blood stream velocity is not high, simple algorithm is used for the modelling of blood stream^{20–23}.

In this work, the blood stream flow profile for inlet is obtained from profile introduced by Boccadifuoco²⁴ (Fig. 2). As displayed in this figure, four distinct points are selection for transient effects of blood pulsatile flow. As shown in this figure, the maximum acceleration (A), peak systole (B), maximum deceleration (C), early diastole (D). The coiling of the model is employed via the porosity inside the aneurysm and the details of selected porosity is obtained from Mitsos et al.²⁵. In this work three main factors of Wall Shear stress (WSS), pressure and OSI are compared in different temporal and operational conditions. OSI is calculated, via following equation:

$$WSS = \mu \left(\frac{\partial u}{\partial y} \right)_{y=0}, \quad (1)$$

$$OSI = \frac{1}{2} \left(1 - \frac{\left| \int_0^T WSS_i dt \right|}{\int_0^T |WSS_i| dt} \right), \quad (2)$$

where u is tangential velocity, t is time, and T is the duration of the cycle.

Computer simulations have been widely used for the simulation of biomechanical devices^{26–32}. Due to inaccessibility, this technique is the best option for analysis of the blood hemodynamic^{33–40}. This The grid generation is also required for the control volume approach^{41–49}. As depicted in Fig. 3, unstructured grid is produced for the selected ICA. For grid independency, we also examined four grids sizes for specific condition and Table 1

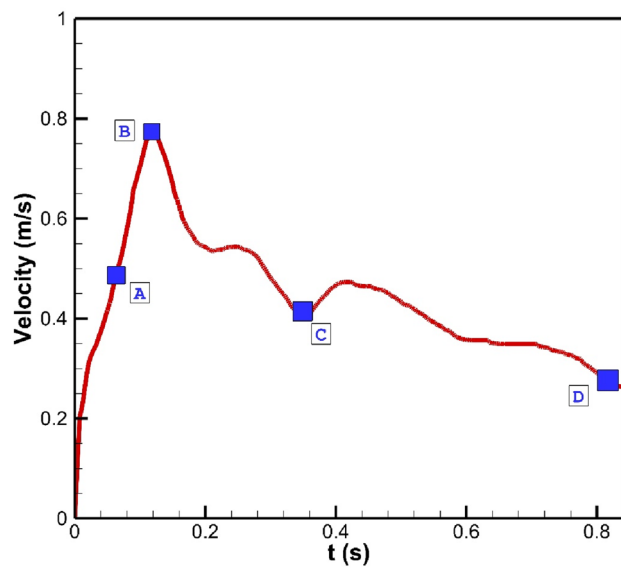


Figure 2. Transient blood flow.

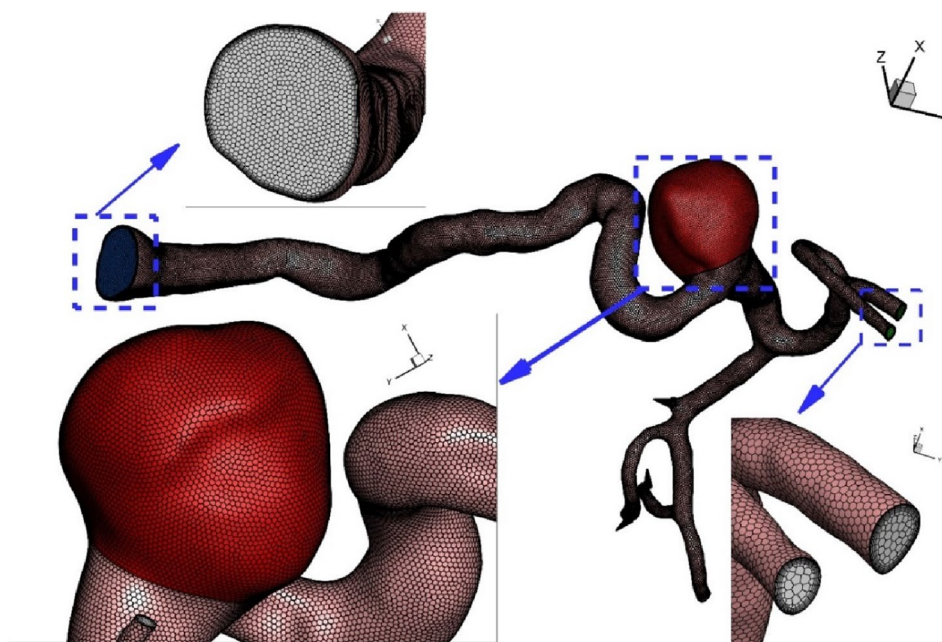


Figure 3. Grid production.

	Cells	Average blood velocity at inlet of sac (maximum acceleration)	Average blood velocity at inlet of sac (peak systolic)
Coarse	722,000	0.342	0.51
medium	1,120,000	0.361	0.54
fine	1,624,000	0.379	0.56
Very fine	2,064,000	0.382	0.561

Table 1. Details of used grids.

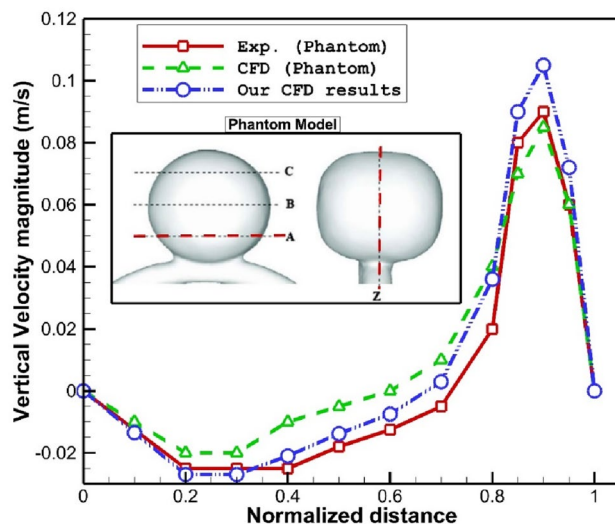


Figure 4. Validation.

demonstrates the impacts of different grids on the velocity magnitude at neck of aneurysm. Finally, fine grid with 1,624,000 cells are chosen for our study.

Results and discussion

To ensure about the results, model developed by Hoi et al.²⁶ is selected for the validation of our method is done. As demonstrated in Fig. 4, the phantom model developed by Hoi et al.²⁶ is simulated and the vertical velocity on the cross-section of plane A and Z are compared with our data. It is found that velocity trend of our results agree well with that of experimental works.

The main attention of this work is to demonstrate the impacts of blood flow pulsation pattern on the main factors i.e. wall shear stress, pressure and OSI on aneurysm wall. Figure 5 demonstrates the wall shear stress on aneurysm wall at four stages of the maximum acceleration (A), peak systole (B), maximum deceleration (C), early diastole (D). The comparison of the AWSS on aneurysm wall in different time instants clearly demonstrates the impacts of the blood mass flow rate on the growth and rupture of the cerebral aneurysm. It is found that the maximum AWSS happens at the maximum of the aneurysm sac. The change of the WSS also indicates that the region with high curvature has maximum wall shear stress. In the following section, we would present more details about the pattern of the WSS change in our selected model.

The OSI value is a reliable factor for the evaluation of the WSS and the detection of high-risk region on the aneurysm wall. Figure 6 demonstrates the growth and change of the OSI in different instants while the blood HCT and coiling porosity are 0.35 and 0.79, respectively. It is noticed that the initiation of high OSI occurs in the neck of aneurysm while it extends into the dome of the aneurysm. The comparison of OSI and WSS contour demonstrates that the maximum OSI occurs in the maximum deceleration while maximum WSS reaches maximum value in peak systolic.

The comparison of the pressure on the aneurysm wall indicates that the angle of blood direction with inlet of sac is highly important for the creation of high-pressure region on sac wall (Fig. 7). The pressure distribution also shows that the incoming blood pressure becomes maximum on the top end of aneurysm sac at peak systolic instant. Besides, the pressure of the blood at neck is high enough to consider this region as high-risk region.

The effects of blood flow rate on the hemodynamic of the blood flow is presented in Fig. 8. In this figure, iso-value of blood velocity magnitude ($u = 0.4$ m/s) is demonstrated to perceive the feature of the blood stream inside the aneurysm sac at different stages in the blood cycle. According to our results, the blood iteration plays main role on the shape of the aneurysm nearby neck.

Due to important of the coiling technique and blood viscosity, we compare these factor on the aneurysm wall in peak systolic condition. Figure 9 illustrates the change of WSS on the aneurysm wall for different coiling porosities (0.79 and 0.89) and blood HCTs of 0.35 and 0.45. Distribution of the WSS confirm that the effects of blood stream on the aneurysm wall declines when the porosity of the coiling is increased. Besides, it is found that the effect of blood viscosity is not substantial on the WSS distribution on the aneurysm wall.

Figure 10 presents quantitative comparison to disclose the effects of coiling and blood haematocrit (HCT) on maximum value of WSS on the aneurysm wall. As expected, maximum value of WSS happens in peak systolic where the effects of coiling are more visible than HCT. In maximum acceleration and deceleration instants, the effects of blood HCT is about 8.5% and found that WSS of female patient (HCT = 0.35) is always lower than that of male (HCT = 0.45).

Due to importance of OSI value, this factor is also compared in these conditions for the chosen ICA. Comparison of OSI for these conditions indicates that there are two high-risk regions on the surface of the aneurysm (as demonstrated by A and B in Fig. 11). Results show that the increasing porosity fraction considerably extends

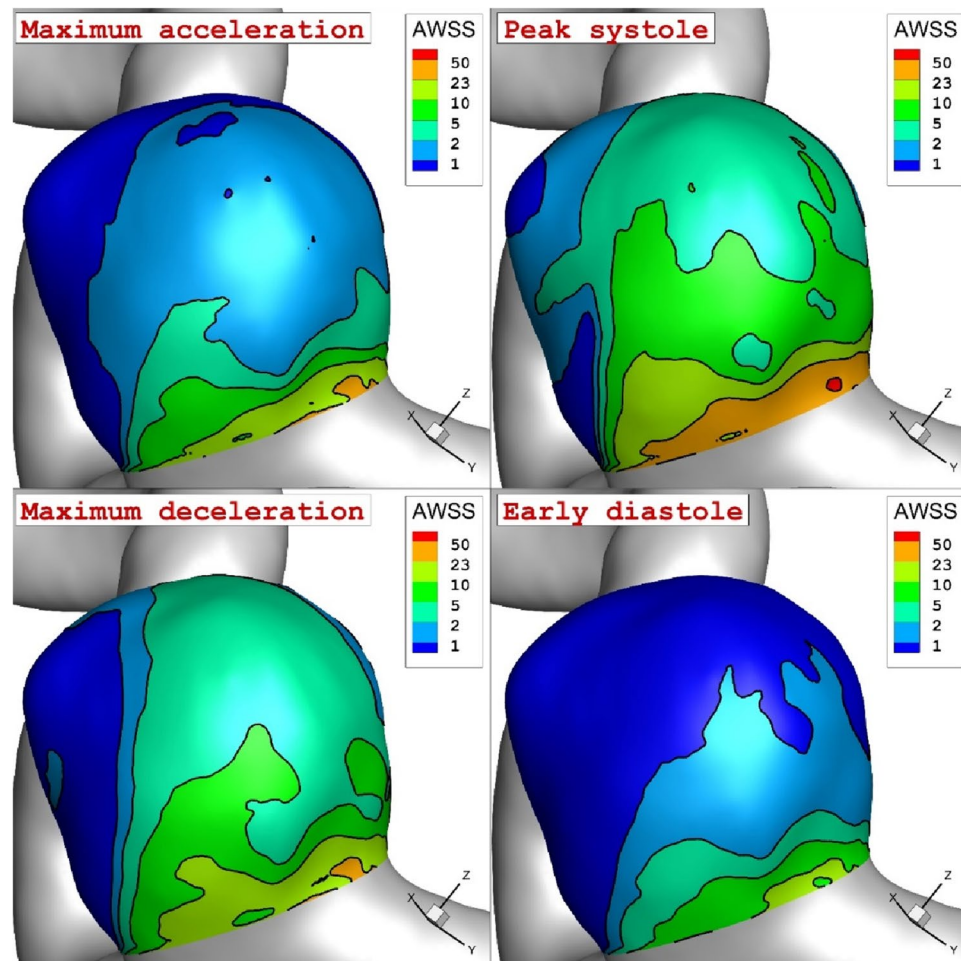


Figure 5. The variation of the WSS on the aneurysm wall in various instants.

zone A while zone B is limited in the same condition. It is observed that increasing the HCT decreases the intensity of the OSI on the wall of the aneurysm.

Quantitative comparison of the maximum OSI also confirm the role of porosity on the reduction of the WSS in different time stages (Fig. 12). In high HCT (HCT = 0.45), changing the porosity of coiling from 0.89 with 0.79 would decline maximum OSI up to 75% (in maximum acceleration). However, this effect is limited to about 45% for the low HCT (HCT = 0.35).

The impact of coiling porosity and blood HCT on the blood iso-velocity are depicted in Fig. 13. The comparison of the blood hemodynamic indicate that the lower porosity (equivalent to higher permeability) considerably limited the blood inflow into the aneurysm sac. Besides, it also declares that the blood viscosity is not effective on blood inflow into the aneurysm. Figure 14 depicts the flow stream inside the aneurysm. The comparison of the flow stream shows that the pressure of incoming blood into the aneurysm decreases in male patients (HCT = 0.45).

Figure 15 illustrates the average velocity entering to the sac of aneurysm in these four conditions. The achieved results indicate that effects of porosity and HCT on the average blood velocity is limited due to geometrical aspects of the selected aneurysm. In fact, the angle of the incoming blood stream with normal of neck face is high and this diminish the impact of aneurysm condition on the velocity of blood inflow.

Conclusion

This work has tried to evaluate the risk of aneurysm rupture for specific ICA in various temporal conditions. Effects of blood pulsate flow on production and growth of the high risk-region. Analyses of wall shear stress, pressure and OSI are done to disclose the hemodynamic effects on the risk of aneurysm rupture. Besides, the effects of coiling and blood viscosity on these factors are also investigated in various conditions. Blood stream inside the aneurysm and shear stress on the wall of the aneurysm are compared for these blood and aneurysm conditions. Our results indicate that blood HCT has limited impact on the growth and rupture of aneurysm while coiling porosity could decrease OSI and WSS about 50% on the aneurysm wall.

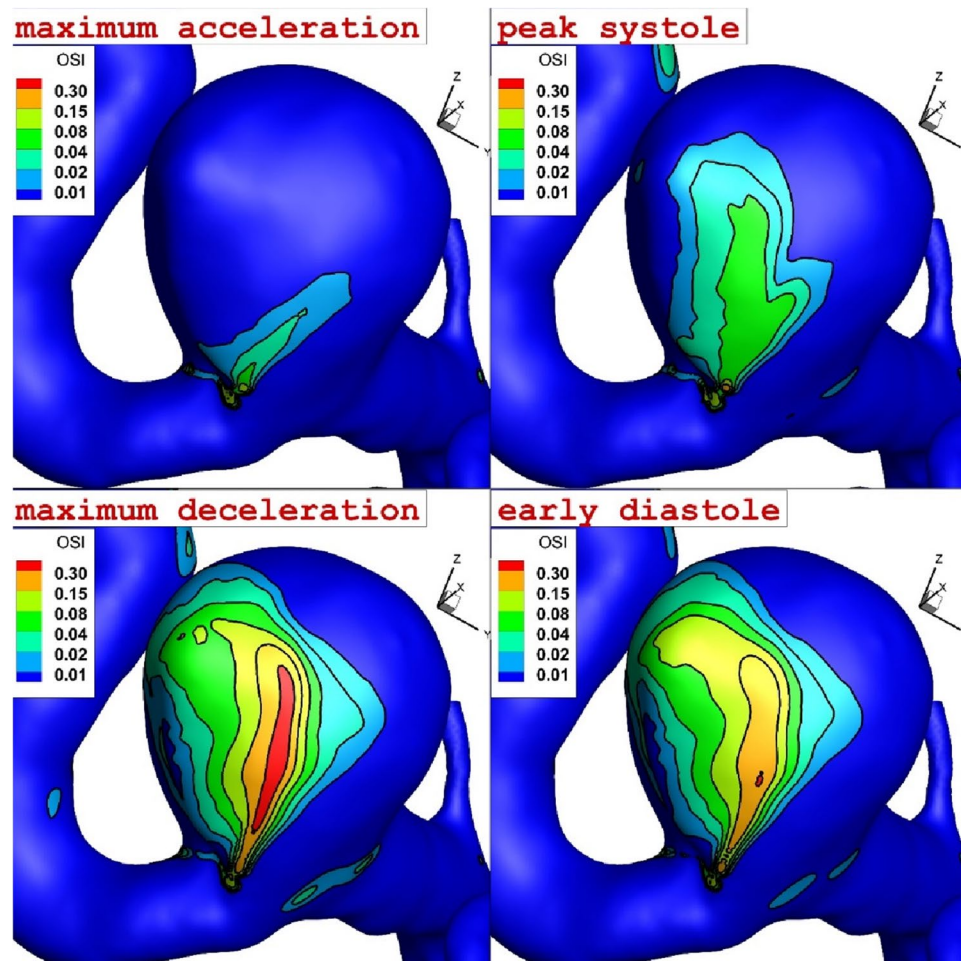


Figure 6. The change of the OSI on the aneurysm wall in four instants of maximum acceleration, peak systolic, maximum deceleration and early diastole.

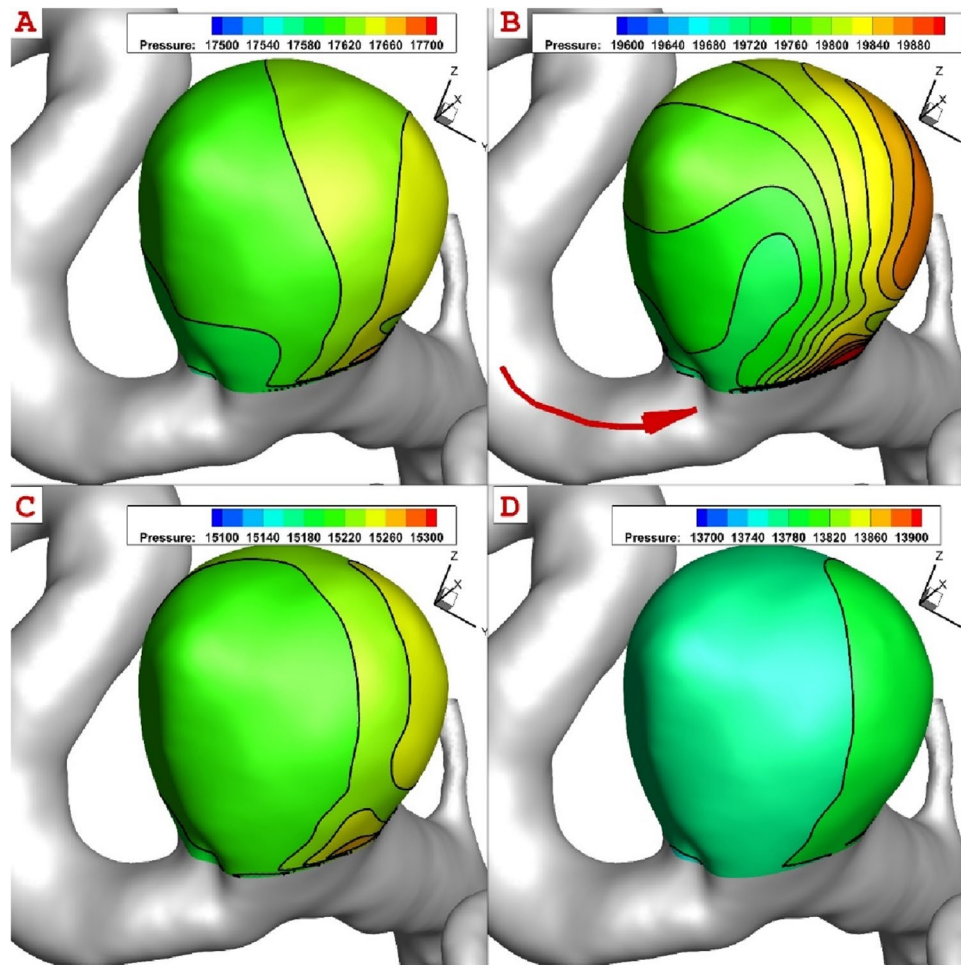


Figure 7. The comparison of the pressure distribution on the aneurysm sac in different instants.

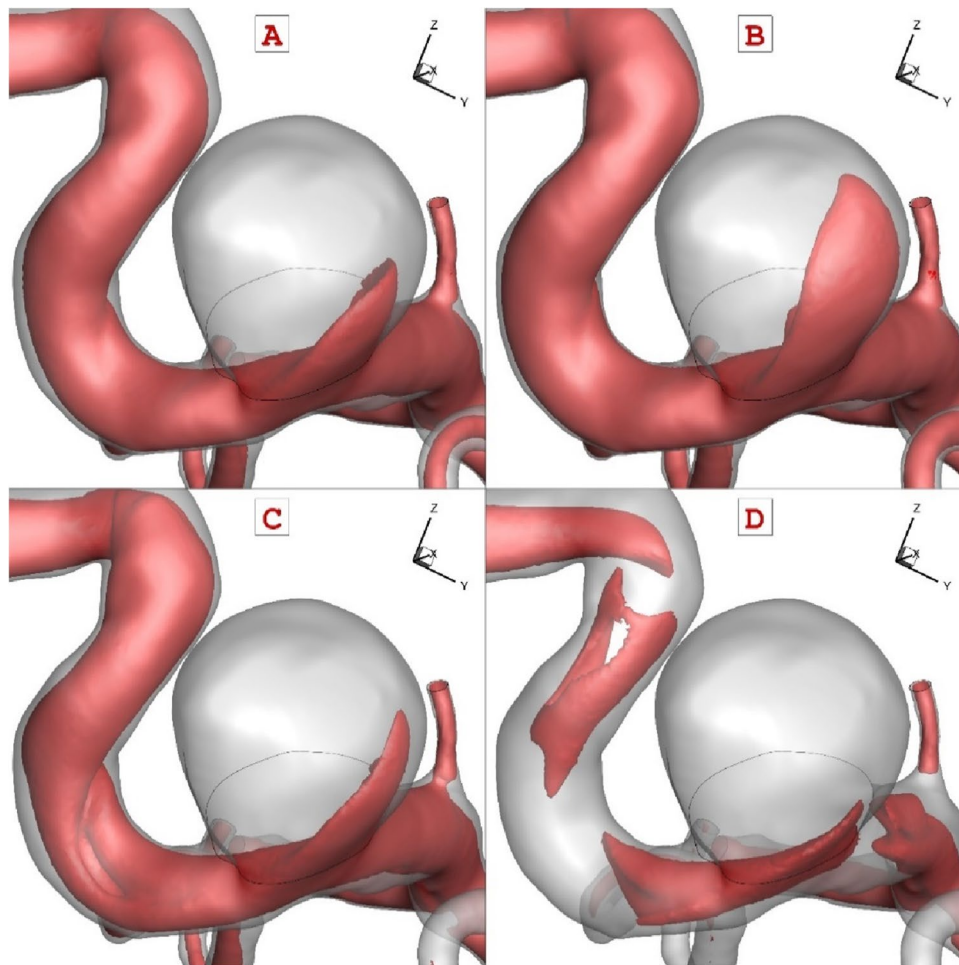


Figure 8. The blood flow feature in various instants (velocity magnitude iso-surface = 0.4 m/s).

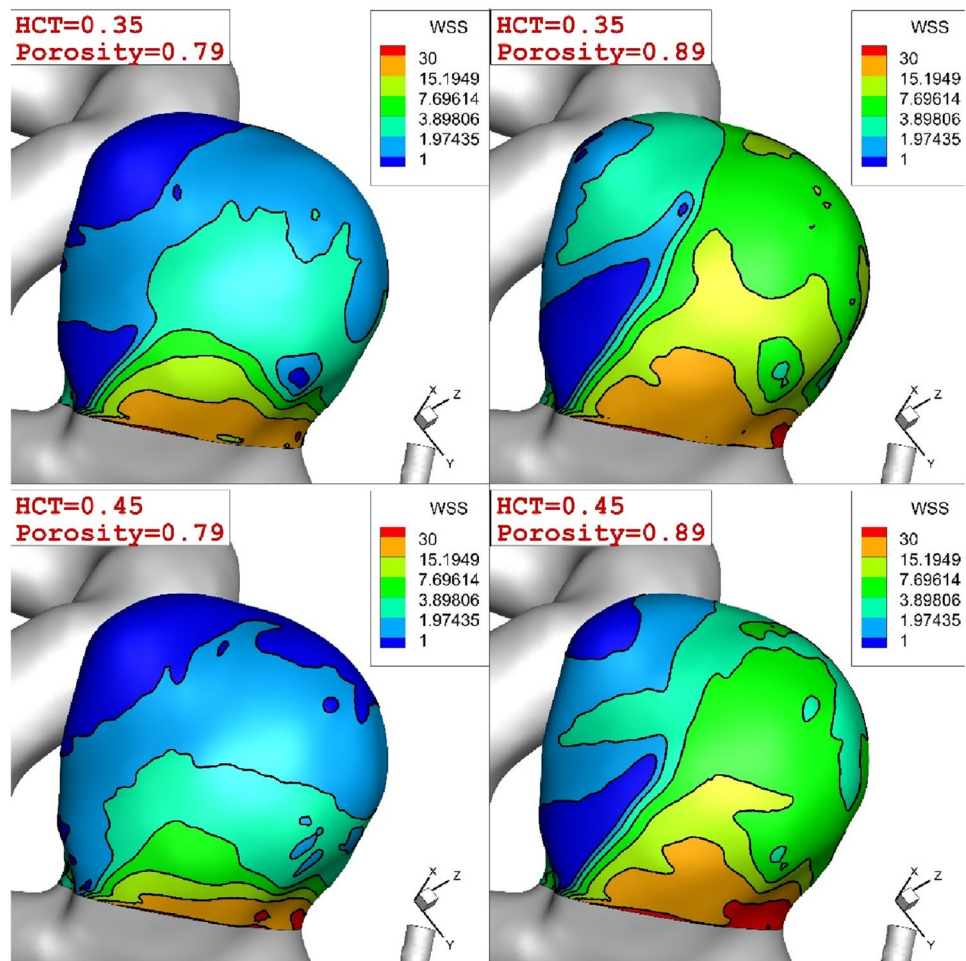


Figure 9. Comparison of the WSS on ICA for different coiling porosities and blood HCTs.

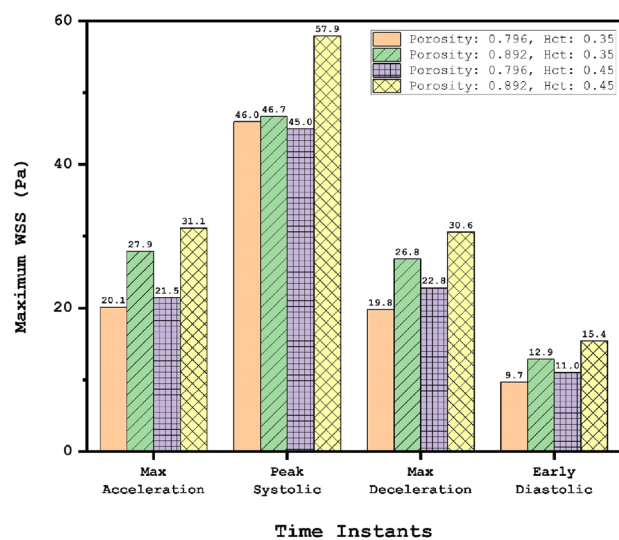


Figure 10. Max WSS (Pa) on Aneurysm in different time instants.

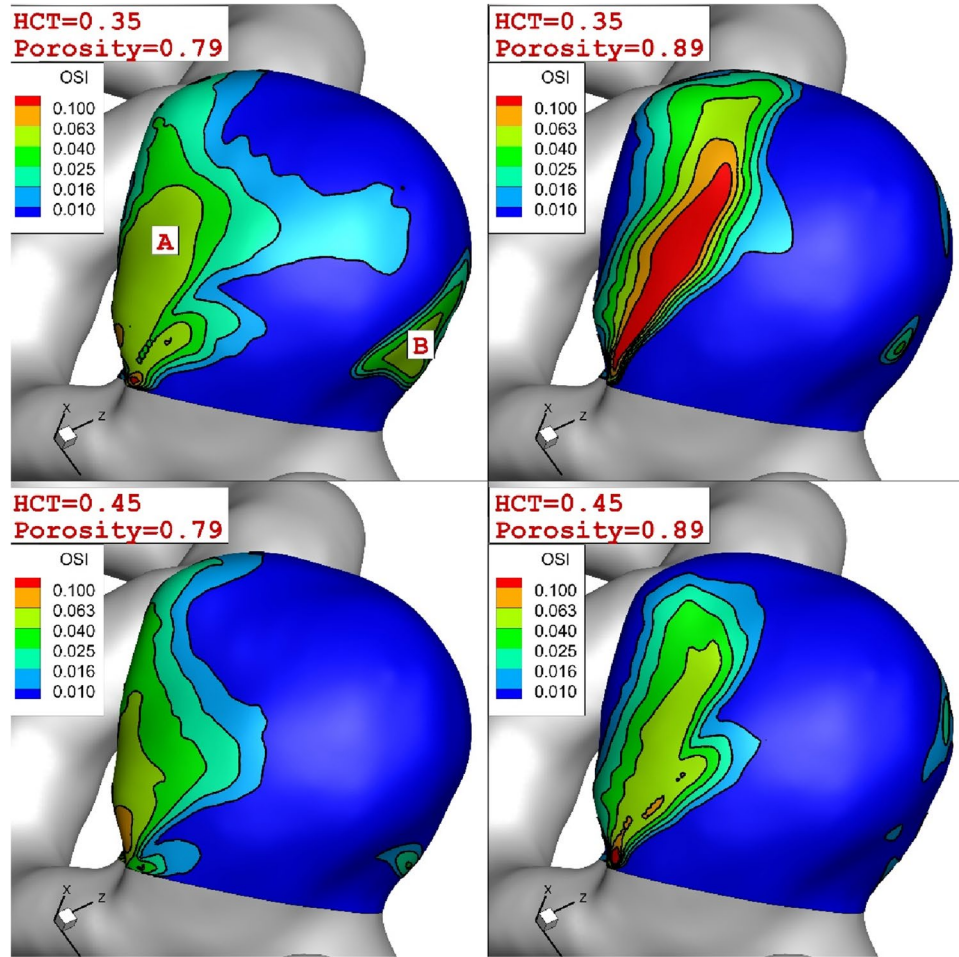


Figure 11. Comparison of the OSI on ICA for different coiling porosities and blood HCTs.

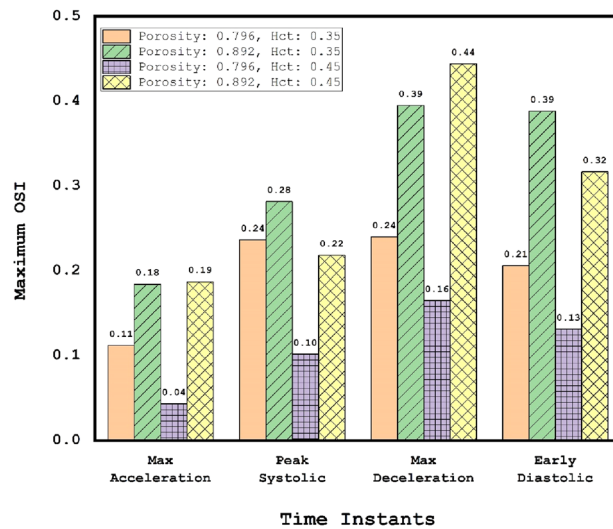


Figure 12. Impacts of coiling porosity and blood HCT on the maximum WSS in different stages.

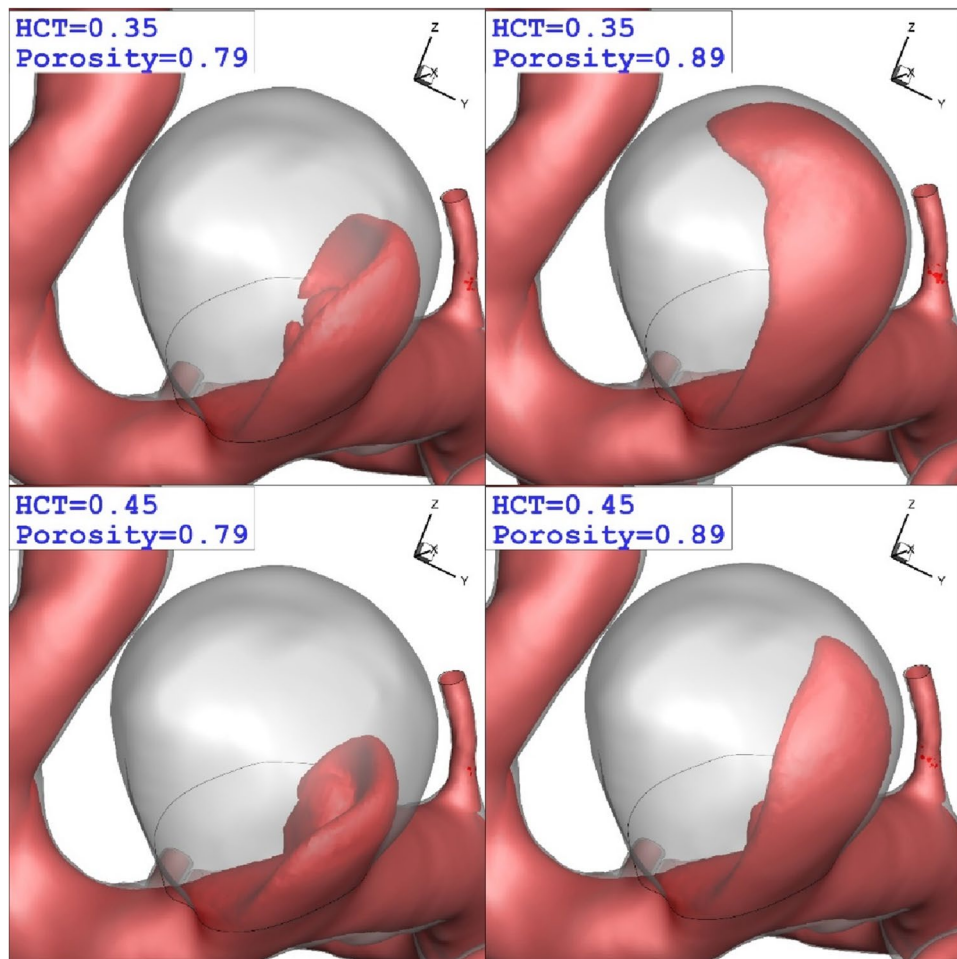


Figure 13. The iso-value of the blood velocity ($u=0.3$ m/s).

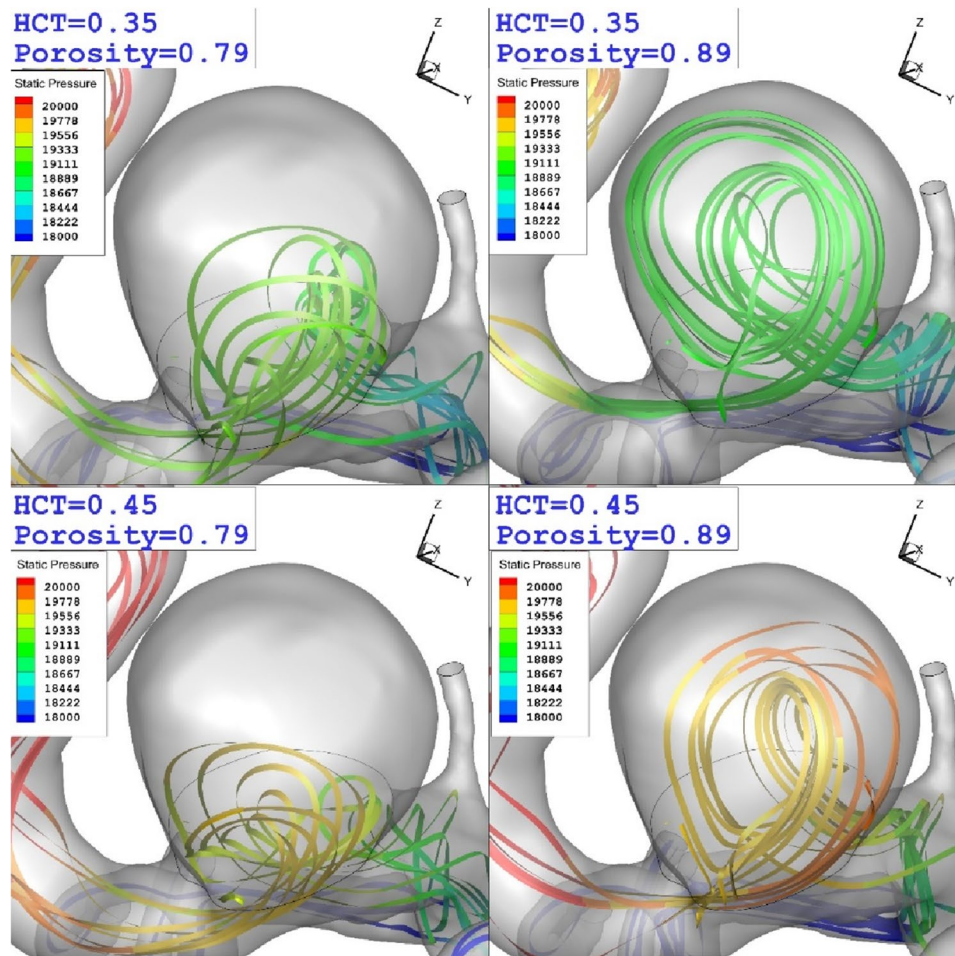


Figure 14. The feature of the blood stream inside aneurysm sac in different coiling porosity and blood HCTs.

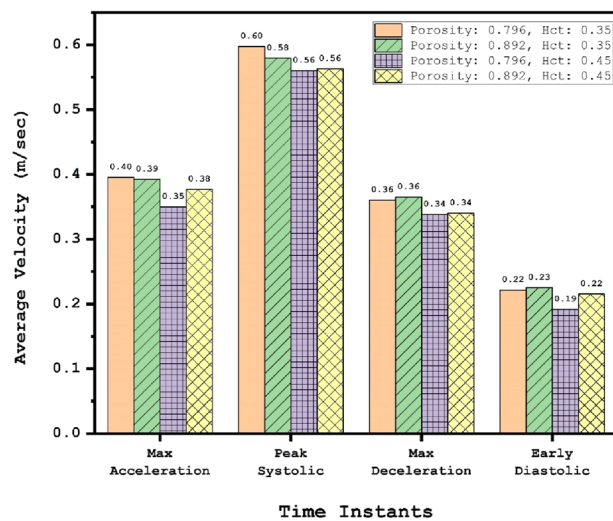


Figure 15. Comparison of the average velocity of the blood flow into the aneurysm sac for different condition and time instants.

Data availability

All data generated or analysed during this study are included in this published article.

Received: 10 August 2022; Accepted: 4 November 2022

Published online: 09 November 2022

References

- Ashkezari, S. F. S. *et al.* Hemodynamics in aneurysm blebs with different wall characteristics. *J. Neuro Interv. Surg.* **13**(7), 642–646 (2021).
- Sforza, D. M., Putman, C. M. & Cebral, J. R. Hemodynamics of cerebral aneurysms. *Annu. Rev. Fluid Mech.* **41**, 91–107 (2009).
- Martu, G., Gasser, T. C., Appoo, J. J. & Di Martino, E. S. Mechano-biology in the thoracic aortic aneurysm: A review and case study. *Biomechan. Model. Mechanobiol.* **13**(5), 917–928 (2014).
- Coady, M. A. *et al.* What is the appropriate size criterion for resection of thoracic aortic aneurysms. *J. Thorac. Cardiovasc. Surg.* **113**(3), 476–491 (1997).
- Abdehkhakha, A. *et al.* Cerebral aneurysm flow diverter modeled as a thin inhomogeneous porous medium in hemodynamic simulations. *Comput. Biol. Med.* **139**, 104988 (2021).
- Lobato, A. C. & Puech-Leao, P. Predictive factors for rupture of thoracoabdominal aortic aneurysm. *J. Vasc. Surg.* **27**(3), 446–453 (1998).
- Elefteriades, J. A. Natural history of thoracic aortic aneurysms: Indications for surgery, and surgical versus nonsurgical risks. *Ann. Thorac. Surg.* **74**(5), S1877–S1880 (2002).
- Pape, L. A. *et al.* Aortic diameter 5.5 cm is not a good predictor of type A aortic dissection: Observations from the International Registry of Acute Aortic Dissection (IRAD). *Circulation* **116**(10), 1120–1127 (2007).
- Celi, S. & Berti, S. Three-dimensional sensitivity assessment of thoracic aortic aneurysm wall stress: A probabilistic finite-element study. *Eur. J. Cardio-thorac. Surg.* **45**(3), 467–475 (2014).
- Zan-Hui Jin, M. Barzegar Gerdroodbary, P. Valipour, M. Faraji, Nidal H. Abu-Hamdeh, CFD investigations of the blood hemodynamic inside internal cerebral aneurysm (ICA) in the existence of coiling embolism *Alexandria Engineering Journal*. <https://doi.org/10.1016/j.aej.2022.10.070> (2023).
- Asal Sadeh, Admin Kazemi, Moharam BahramKhou, M. Barzegar Gerdroodbary, Computational analysis of the blood hemodynamic inside internal cerebral aneurysm in the existence of endovascular coiling, *International j of modern physic C*. <https://doi.org/10.1142/S0129183123500596> (2023).
- Gallo, D. *et al.* On the use of in vivo measured flow rates as boundary conditions for image-based hemodynamic models of the human aorta: Implications for indicators of abnormal flow. *Ann. Biomed. Eng.* **40**(3), 729–741 (2012).
- Martu, G., Forneris, A., Appoo, J. J. & Di Martino, E. S. Is there a role for biomechanical engineering in helping to elucidate the risk profile of the thoracic aorta?. *Ann. Thorac. Surg.* **101**(1), 390–398 (2016).
- Shen, X.-Y., Barzegar Gerdroodbary, M., Poozesh, A., Abazari, A. M. & Imani, S. M. Effects of blood flow characteristics on rupture of cerebral aneurysm: Computational study. *Int. J. Mod. Phys. C* **32**(11), 2150143 (2021).
- Shen, X.-Y., Gerdroodbary, M. B., Abazari, A. M. & Moradi, R. Computational study of blood flow characteristics on formation of the aneurysm in internal carotid artery. *Eur. Phys. J. Plus* **136**(5), 541 (2021).
- Shen, X.-Y. *et al.* Numerical simulation of blood flow effects on rupture of aneurysm in middle cerebral artery. *Int. J. Mod. Phys. C* **33**(03), 2250030 (2022).
- Fung, Y. C. *Biomechanics: Mechanical Properties of Living Tissues* 2nd edn. (Springer, 1993).
- Razavi, A., Shirani, E. & Sadeghi, M. Numerical simulation of blood pulsatile flow in a stenosed carotid artery using different rheological models. *J. Biomech.* **44**, 2021–2030 (2011).
- AneuriskWeb project website. <http://ecm2.mathcs.emory.edu/aneuriskweb>. Emory University, Department of Math&CS (2012).
- Malvè, M. *et al.* Impedance-based outflow boundary conditions for human carotid haemodynamics. *Comput. Methods Biomech. Biomed. Eng.* **17**(11), 1248–1260 (2014).
- Voss, S., Beuing, O., Janiga, G. & Berg, P. Stent-induced vessel deformation after intracranial aneurysm treatment—A hemodynamic pilot study. *Comput. Biol. Med.* **111**, 103338 (2019).
- Qin, S. *et al.* Efficient parallel simulation of hemodynamics in patient-specific abdominal aorta with aneurysm. *Comput. Biol. Med.* **136**, 104652 (2021).
- Xu, L., Liang, F., Zhao, B., Wan, J. & Liu, H. Influence of aging-induced flow waveform variation on hemodynamics in aneurysms present at the internal carotid artery: A computational model-based study. *Comput. Biol. Med.* **101**, 51–60 (2018).
- Boccafio, A., Mariotti, A., Celi, S., Martini, N. & Salvetti, M. V. Impact of uncertainties in outflow boundary conditions on the predictions of hemodynamic simulations of ascending thoracic aortic aneurysms. *Comput. Fluids* **165**, 96–115 (2018).
- Mitsos, A. P., Kakalis, N. M. P., Ventikos, Y. P. & Byrne, J. V. Haemodynamic simulation of aneurysm coiling in an anatomically accurate computational fluid dynamics model. *Neuroradiology* **50**(4), 341–347 (2008).
- Hoi, Y., Woodward, S. H., Kim, M., Taulbee, D. B. & Meng, H. Validation of CFD simulations of cerebral aneurysms with implications of geometric variations. *J. Biomech. Eng.* **128**(6), 844–851. <https://doi.org/10.1115/1.2354209> (2006).
- Hou, Q., Huang, J., Xiong, X., Guo, Y. & Zhang, B. Role of nutrient-sensing receptor GPR6A in regulating colonic group 3 innate lymphoid cells and inflamed mucosal healing. *J. Crohns Colitis* <https://doi.org/10.1093/ecco-jcc/jjac020> (2022).
- Zhuo, Z. *et al.* A loop-based and AGO-incorporated virtual screening model targeting AGO-mediated miRNA–mRNA interactions for drug discovery to rescue bone phenotype in genetically modified mice. *Adv. Sci.* **7**(13), 1903451. <https://doi.org/10.1002/adv.201903451> (2020).
- Yan, J. *et al.* Chiral protein supraparticles for tumor suppression and synergistic immunotherapy: An enabling strategy for bioactive supramolecular chirality construction. *Nano Lett.* **20**(8), 5844–5852. <https://doi.org/10.1021/acs.nanolett.0c01757> (2020).
- Yang, W., Liu, W., Li, X., Yan, J. & He, W. Turning chiral peptides into a racemic supraparticle to induce the self-degradation of MDM2. *J. Adv. Res.* <https://doi.org/10.1016/j.jare.2022.05.009> (2022).
- Jin, K. *et al.* Multimodal deep learning with feature level fusion for identification of choroidal neovascularization activity in age-related macular degeneration. *Acta Ophthalmol. (Oxford, England)* **100**(2), e512–e520. <https://doi.org/10.1111/aos.14928> (2022).
- Li, Z. *et al.* Sb-doped WO₃ based QCM humidity sensor with self-recovery ability for real-time monitoring of respiration and wound. *Sens. Actuators B. Chem.* <https://doi.org/10.1016/j.snb.2022.131691> (2022).
- Liu, C. *et al.* Engineered extracellular vesicles and their mimetics for cancer immunotherapy. *J. Control. Release* **349**, 679–698. <https://doi.org/10.1016/j.jconrel.2022.05.062> (2022).
- Zhang, X. *et al.* Gestational leucylation suppresses embryonic T-box transcription factor 5 signal and causes congenital heart disease. *Adv. Sci.* **9**(15), 2201034. <https://doi.org/10.1002/adv.202201034> (2022).
- Cai, K. *et al.* Nicotinamide mononucleotide alleviates cardiomyopathy phenotypes caused by short-chain enoyl-CoA hydratase 1 deficiency. *JACC Basic Transl. Sci.* **7**(4), 348–362. <https://doi.org/10.1016/j.jacbts.2021.12.007> (2022).
- Zhang, X. *et al.* Homocysteine inhibits pro-insulin receptor cleavage and causes insulin resistance via protein cysteine-homocysteinylolation. *Cell Rep.* **37**(2), 109821. <https://doi.org/10.1016/j.celrep.2021.109821> (2021).

37. Wang, X. *et al.* Low chorionic villous succinate accumulation associates with recurrent spontaneous abortion risk. *Nat. Commun.* **12**(1), 3428. <https://doi.org/10.1038/s41467-021-23827-0> (2021).
38. Xu, S. *et al.* Ketogenic diets inhibit mitochondrial biogenesis and induce cardiac fibrosis. *Signal Transduct. Target. Ther.* **6**(1), 54. <https://doi.org/10.1038/s41392-020-00411-4> (2021).
39. Qu, Y. *et al.* Inactivation of the AMPK–GATA3–ECHS1 pathway induces fatty acid synthesis that promotes clear cell renal cell carcinoma growth. *Cancer Res.* **80**(2), 319–333. <https://doi.org/10.1158/0008-5472.CAN-19-1023> (2020).
40. Li, Y. *et al.* APC/CCDH1 synchronizes ribose-5-phosphate levels and DNA synthesis to cell cycle progression. *Nat. Commun.* **10**(1), 2502. <https://doi.org/10.1038/s41467-019-10375-x> (2019).
41. Wang, D. *et al.* Colonic lysine homocysteinylation induced by high-fat diet suppresses DNA damage repair. *Cell Rep.* **25**(2), 398–412. <https://doi.org/10.1016/j.celrep.2018.09.022> (2018).
42. Wang, D. *et al.* Lower circulating folate induced by a fidgetin intronic variant is associated with reduced congenital heart disease susceptibility. *Circulation* **135**(18), 1733–1748. <https://doi.org/10.1161/circulationaha.116.025164> (2017).
43. Song, K. & Wu, D. Shared decision-making in the management of patients with inflammatory bowel disease. *World J. Gastroenterol.* **28**(26), 3092–3100. <https://doi.org/10.3748/wjg.v28.i26.3092> (2022).
44. Duan, C. *et al.* Accelerate gas diffusion-weighted MRI for lung morphometry with deep learning. *Eur. Radiol.* **32**(1), 702–713. <https://doi.org/10.1007/s00330-021-08126-y> (2022).
45. Li, H. *et al.* Damaged lung gas exchange function of discharged COVID-19 patients detected by hyperpolarized ¹²⁹Xe MRI. *Sci. Adv.* **7**(1), e8180. <https://doi.org/10.1126/sciadv.abc8180> (2021).
46. Zeng, Q. *et al.* Hyperpolarized Xe NMR signal advancement by metal-organic framework entrapment in aqueous solution. *Proc. Natl. Acad. Sci.* **117**(30), 17558–17563. <https://doi.org/10.1073/pnas.2004121117> (2020).
47. Zou, M. *et al.* Gut microbiota on admission as predictive biomarker for acute necrotizing pancreatitis. *Front. Immunol.* **13**, 988326. <https://doi.org/10.3389/fimmu.2022.988326> (2022).
48. Hao, P. *et al.* Serum metal ion-induced cross-linking of photoelectrochemical peptides and circulating proteins for evaluating cardiac ischemia/reperfusion. *ACS Sens.* **7**(3), 775–783. <https://doi.org/10.1021/acssensors.1c02305> (2022).
49. Liu, Q., Peng, H. & Wang, Z. Convergence to nonlinear diffusion waves for a hyperbolic–parabolic chemotaxis system modelling vasculogenesis. *J. Differ. Equ.* **314**, 251–286. <https://doi.org/10.1016/j.jde.2022.01.021> (2022).

Author contributions

S.S. and M.B.G. wrote the main manuscript text. A.S. and A.P. prepared Figs. 1, 2, 3. A.H. and A.Sh. revised the manuscript. All authors reviewed the manuscript.

Competing interests

The authors declare no competing interests.

Additional information

Correspondence and requests for materials should be addressed to M..B.G.

Reprints and permissions information is available at www.nature.com/reprints.

Publisher's note Springer Nature remains neutral with regard to jurisdictional claims in published maps and institutional affiliations.



Open Access This article is licensed under a Creative Commons Attribution 4.0 International License, which permits use, sharing, adaptation, distribution and reproduction in any medium or format, as long as you give appropriate credit to the original author(s) and the source, provide a link to the Creative Commons licence, and indicate if changes were made. The images or other third party material in this article are included in the article's Creative Commons licence, unless indicated otherwise in a credit line to the material. If material is not included in the article's Creative Commons licence and your intended use is not permitted by statutory regulation or exceeds the permitted use, you will need to obtain permission directly from the copyright holder. To view a copy of this licence, visit <http://creativecommons.org/licenses/by/4.0/>.

© The Author(s) 2022